

## Hot Deformation Behavior of 17-7 PH Stainless Steel

M. Zeinali<sup>1</sup>, E. Shafiei<sup>2\*</sup>, R. Hosseini<sup>3</sup>, Kh. Farmanesh<sup>1</sup>, A.R. Soltanipoor<sup>1</sup> and E. Maghsodi<sup>1</sup>

<sup>1</sup>Department of Materials Science and Engineering, Maleke Ashtar University of Technology, Shahin Shahr, Iran.

<sup>2</sup>Department of Mining and Metallurgical Engineering, Amirkabir University of Technology, Tehran, Iran.

<sup>3</sup>Department of Materials Science and Engineering, Shiraz University, Shiraz, Iran.

**Abstract:** To investigate the hot deformation behavior of 17-7 PH stainless steel, hot compression tests were carried out at the temperatures of 950, 1050 and 1150 °C and strain rates of 0.001 s<sup>-1</sup> to 0.1 s<sup>-1</sup>. Accordingly, the hot working behavior was studied by the analyses of flow stress curves, work hardening rate versus stress curves, exponent- type constitutive equations and deformed microstructures. Meanwhile, the average normalized critical stress for initiation of dynamic recrystallization (DRX) was determined using a 3<sup>rd</sup> order polynomial curve fitting. The results show that the flow stress depends strongly on the deformation temperature and the strain rate, and it increases with decreasing the deformation temperature and increasing the strain rate. Furthermore, it was found out that the co- existence of  $\delta$ - ferrite lowers the softening rate at high Z (Zener- Holloman parameter) conditions. The experimental results were then used to determine the constants of constitutive equations. There is a good agreement between the measured and predicted results indicating a high accuracy of exponent- type constitutive equations.

**Keywords:** Hot deformation, Dynamic recrystallization, Constitutive analysis, 17-7 PH stainless steel

### 1. Introduction

Hot deformation processing of steels, which is usually conducted in the stability range corresponding to the austenite phase, plays an important role in industry for the production of steels with a number of desirable mechanical properties while keeping production costs as low as possible. In order to achieve this goal, the parameters of the forming process must be carefully controlled. An understanding of the microstructural behavior of the steel under consideration is therefore required, together with the constitutive analysis describing material flow [1,2].

Moreover, several interconnected metallurgical phenomena such as work hardening, dynamic recovery (DRV), dynamic recrystallization (DRX), etc., occur during high temperature deformation of materials. In high stacking fault energy (SFE) materials such as aluminum alloys, DRV can balance work hardening, and a plateau is achieved in stress [3]. However, in austenitic steels with lower SFE, the kinetics of DRV is lower, and DRX can be initiated at a critical condition of stress accumulation [4]. The occurrence of DRX leads to grain refinement and reduction in deformation resistance [5]. The general descriptive model for DRX is that the nucleation of DRX grains can start at a critical strain which is a function of initial microstructure and deformation conditions. Then, the evolution of DRX microstructure can proceed further by increasing deformation and through the formation of a necklace structure [6]. Considerable research on DRX kinetics have focused on measuring by metallographic images or EBSD maps of the frozen microstructures at different deformation conditions such as temperature, strain rate, and amount of plastic deformation [7-10]. Meanwhile, the relationships between microstructure variations and deformation parameters are analyzed at different levels. For austenitic steels such as 17-7 PH, a

pronounced interaction between DRX evolution and mechanical property is implicit in flow behavior. Thus, it is realizable to model DRX evolution by analyzing the true stress- strain curves.

The objective of this study is to establish the relationship between the flow stress, strain, strain rate, and temperature to predict the high temperature flow behavior of 17-7 PH. Toward this end, hot compression tests were conducted in a wide range of strain rates and temperatures. The experimental stress- strain data were then employed to derive a constitutive equation relating flow stress, strain rate, and temperature. The critical stress for initiation of dynamic recrystallization was determined using Najafizadeh and Jonas [8,9] method, as well.

## 2. Experimental Procedures

A 17-7 PH stainless steel with chemical composition of 0.04 wt% C- 17.49 wt% Cr- 7.15 wt% Ni- 0.3 wt% Cu- 0.74 wt% Mn was used in this work. The base material was homogenized at temperature of 1050 °C for 1 hr and, then the specimens with height of 18mm and diameter of 12mm were prepared using electron discharge machine (EDM). The hot compression tests were conducted on Z250 Zwick/Roell thermo-mechanical simulator at temperatures of 950, 1050 and 1150 °C and strain rates of 0.001, 0.01 and 0.1 s<sup>-1</sup>. All the specimens were then frozen to study the microstructure. Electrolyte etching with 60% aqueous nitric acid at 1.5 V DC for 60- 120 seconds revealed the grain boundaries.

## 3. Results and Discussion

### 3.1. Effect of deformation conditions on flow stress curves

Flow stress curves obtained at different temperatures and strain rates are shown in Fig. 1. Most of the curves exhibit typical DRX behavior with a single peak stress followed by a gradual fall towards a steady-state stress. However, the peak becomes less obvious when the strain rate increases or the deformation temperature decreases. The drop in flow stress with deformation temperature may be attributed to the increase in the rate of restoration mechanisms and decrease in the work hardening rate. Since the formation of DRX nuclei becomes easier at higher deformation temperatures, the critical strain for initiation of DRX decreases. Moreover, the mobility of grain boundaries increases with increasing deformation temperature and hence the rate of DRX increases. Therefore, both the peak and steady state strains decrease with increasing the deformation temperature [4]. The increase in the flow stress with strain rate can be ascribed to the decrease in the rate of restoration mechanisms and increase in work hardening rate. The rate of DRV also decreases with increasing strain rates. Since the formation of DRX nuclei depends on the recovery substructures, the increase in the critical strain for initiation of DRX with increasing strain rate is reasonable. Moreover, the mobility of grain boundaries decreases with increasing strain rate, which in turn increases the peak and steady state strains [4, 9].

It should be noted that the flow stress drops slowly with increasing the strain after the peak stress, indicating that the process of DRX for the studied alloy is rather sluggish. This can be ascribed to the high alloying elements in austenite which can change the stacking fault energy and grain boundary mobility, leading to accelerate the recovery process [10]. Furthermore, the co-existence of  $\delta$ - ferrite may cause strain in- homogeneity due to different restoration processes and this can lower ductility [11]. Accordingly, at high Z (Zener- Hollomon parameter) conditions the stress decreases continuously to the rupture of the sample before achieving the steady state stress.

### 3.2. Effect of deformation conditions on DRX microstructures

Microstructures obtained at different deformation conditions are shown in Figs. 2 and 3. These figures show that the average dynamically recrystallized grain size increases with increasing the deformation temperature. This increase could be attributed to the decrease in work hardening rate and also to the increase in the mobility of grain boundaries and hence the growth rate. By the way, As shown in Figs. 2 and 3, the average dynamically recrystallized grain size decreases with increasing strain rate. This

decrease could be ascribed to the decrease in grain boundary mobility and grain growth rate at high strain rates. Meanwhile, the percentage of  $\delta$ -ferrite seems to be approximately constant at different deformation conditions which causes lower rate of softening at high Z conditions.

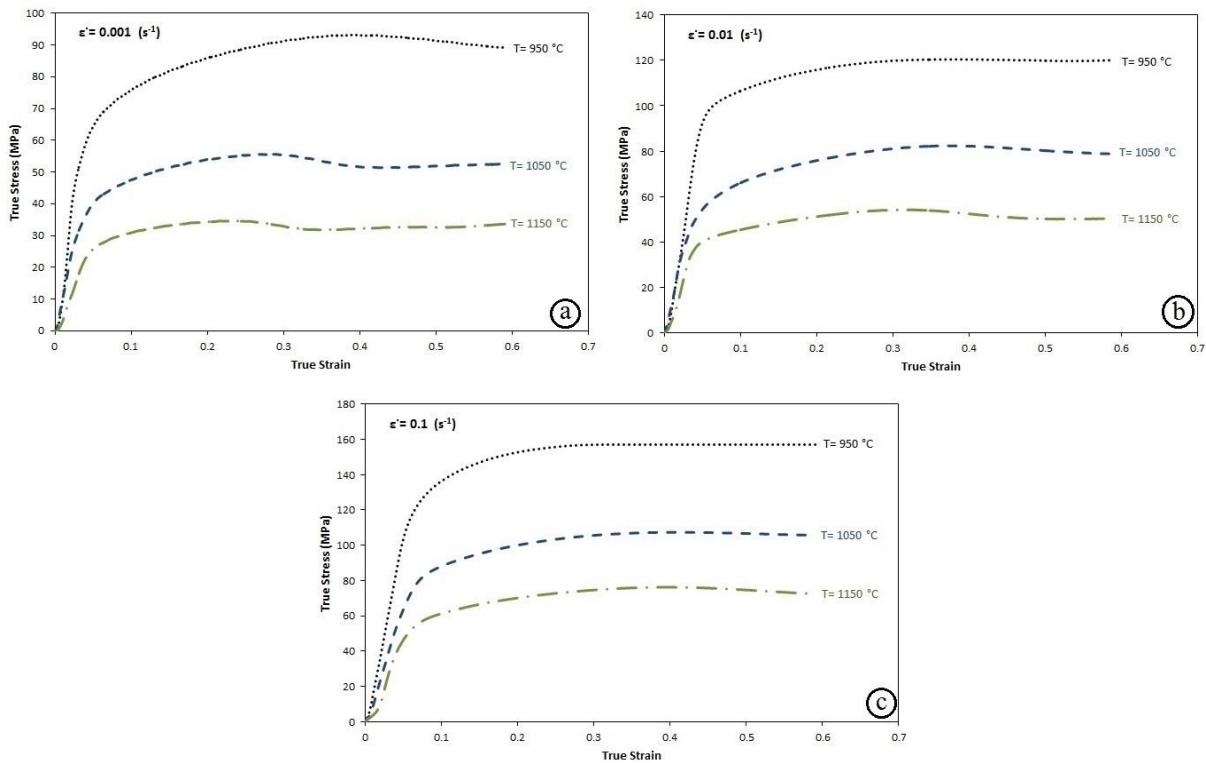


Fig. 1. Flow stress curves obtained at different deformation conditions (a)  $0.001 \text{ S}^{-1}$  (b)  $0.01 \text{ S}^{-1}$  (c)  $0.1 \text{ S}^{-1}$ .

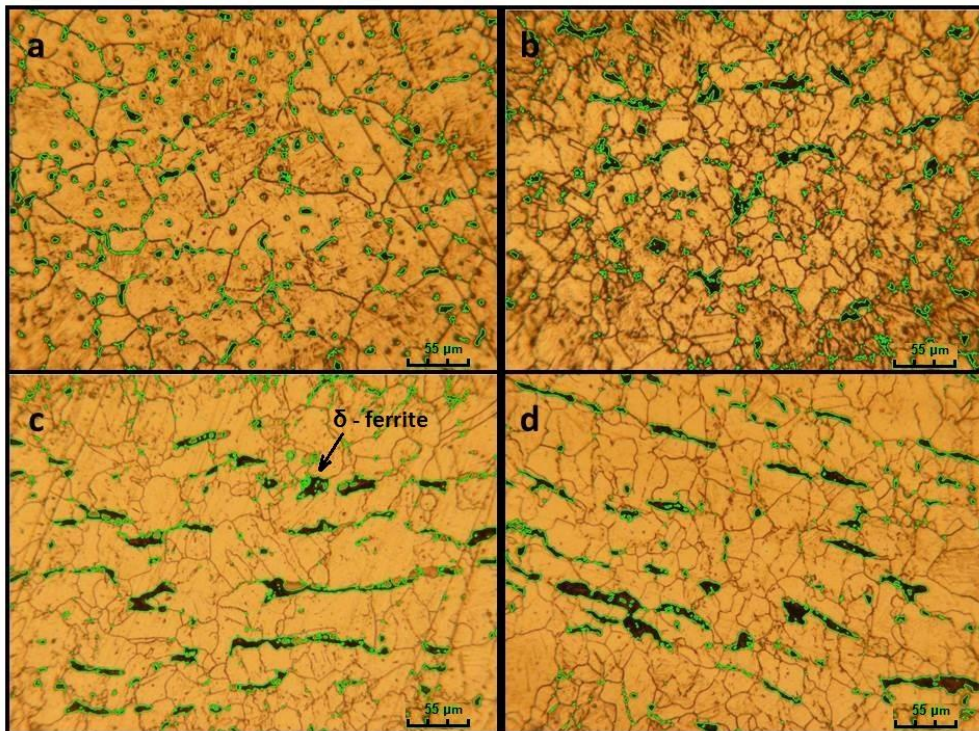


Fig. 2. Optical micrograph of hot compressed 17-7 PH alloy at different deformation conditions (a) annealed (b)  $0.001 \text{ S}^{-1} - 1050 \text{ °C}$  (c)  $0.01 \text{ S}^{-1} - 1050 \text{ °C}$  (d)  $0.1 \text{ S}^{-1} - 1050 \text{ °C}$ .

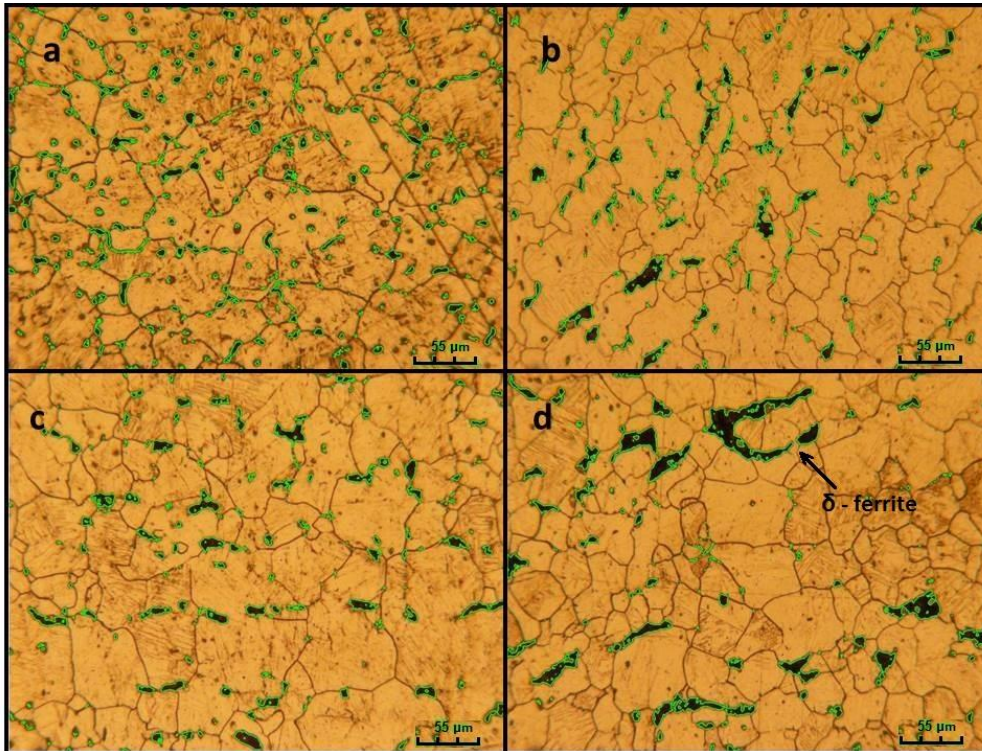


Fig. 3. Optical micrograph of hot compressed 17-7 PH alloy at different deformation conditions (a) annealed (b)  $0.001 \text{ S}^{-1} - 1150 \text{ }^{\circ}\text{C}$  (c)  $0.01 \text{ S}^{-1} - 1150 \text{ }^{\circ}\text{C}$  (d)  $0.1 \text{ S}^{-1} - 1150 \text{ }^{\circ}\text{C}$ .

### 3.3. Work hardening rate versus stress

The change in the slope ( $\Theta = d\sigma/d\varepsilon$ ) of the stress-strain curve with stress can be a good indication of the microstructural changes taking place in material [12,13]. All of the  $\Theta$ - $\sigma$  curves for a particular alloy originate from a common intercept  $\Theta_0$  at  $\sigma=0$ . The  $\Theta$ - $\sigma$  curves have three segments, two of them are linear. The first linear segment decreases with stress for initial strain to the point where sub grains begin to form with a lower rate of increase in DRV. The curve gradually changes to the lower slope of the second linear segment up to the point where the critical stress  $\sigma_c$  is attained for initiating the dynamic recrystallization. The curve then drops off rather sharply to  $\Theta=0$  at peak stress. Fig. 4 shows  $\theta$ - $\sigma$  curves of 17-7 PH alloy at different deformation conditions and its corresponding minimum in  $-d\theta/d\sigma$  curve for a typical deformation condition which approves the occurrence of DRX. The values of critical stress were then determined using the  $\theta$ - $\sigma$  curves.

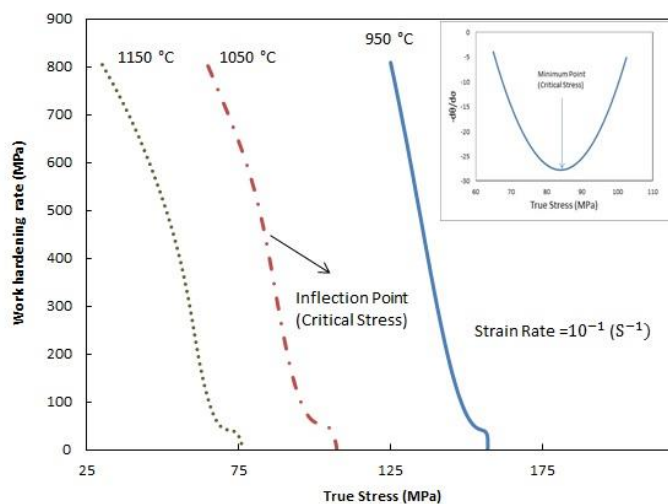


Fig. 4.  $\theta$ - $\sigma$  curves of 17-7 PH steel at different deformation conditions.

### 3.3.1. Determination of critical stress for initiation of DRX

Several attempts have been made to predict the initiation of DRX. For example, Ryan and McQueen observed that the presence of a stress peak at a constant strain rate flow curve leads to an inflection in plots of strain hardening rate,  $\theta$ , versus stress,  $\sigma$  [12,14]. Moreover, the points of inflection in  $\theta$ - $\sigma$  plots where the experimental curves separate from the extrapolated lower linear segments give critical conditions for initiation of DRX (as shown in Fig. 4). Later, Poliak and Jonas [15] have shown that this inflection point corresponds to the appearance of an additional thermodynamic degree of freedom in the system due to the initiation of DRX.

The simple method of Najafizadeh and Jonas [8,9] was used for determination of the critical stress for initiation of DRX. The inflection point is detected by fitting a third order polynomial to the  $\theta$ - $\sigma$  curves up to the peak point as follows:

$$\theta = A\sigma^3 + B\sigma^2 + C\sigma + D \quad (1)$$

where  $A$ ,  $B$ ,  $C$ , and  $D$  are constants for a given set of deformation conditions. The second derivative of this equation with respect to  $\sigma$  can be expressed as:

$$\frac{d^2\theta}{d\sigma^2} = 6A\sigma + 2B \quad (2)$$

At critical stress for initiation of DRX represented as the inflection point, the second derivative becomes zero. Therefore,

$$6A\sigma + 2B = 0 \rightarrow \sigma_c = -\frac{2B}{6A} \quad (3)$$

Table 1 shows the third order polynomial equations of  $\theta$ - $\sigma$  curves at different deformation conditions. As can be seen, the third order curves have a good fit as previously demonstrated by Najafizadeh and Jonas [8,9]. Therefore, this method was used to determine the value of critical stress at different deformation conditions. According to Fig. 5, the normalized critical stress could be expressed as:

$$\sigma_c / \sigma_p = 0.747 \quad (4)$$

Table 1. 3<sup>rd</sup> order polynomial equation of  $\theta$ - $\sigma$  curves at different deformation conditions

Temperature (°C)	Strain rate (S <sup>-1</sup> )	3 <sup>rd</sup> Polynomial curve fitting	R <sup>2</sup>	Critical stress (MPa)	Peak stress (MPa)
950	0.1	$\theta = 0.0199 \sigma^3 - 7.9053 \sigma^2 + 1010.3 \sigma - 40901$	0.99	129.16	157
1050	0.001	$\theta = 0.0609 \sigma^3 - 7.2158 \sigma^2 + 247.38 \sigma - 1882$	0.99	39.5	55.5
1050	0.01	$\theta = 0.0071 \sigma^3 - 0.9287 \sigma^2 + 10.832 \sigma + 1486.9$	0.98	43.5	82.2
1050	0.1	$\theta = 0.0219 \sigma^3 - 5.5176 \sigma^2 + 435.58 \sigma - 10217$	0.99	83.9	107.1
1150	0.001	$\theta = -0.0291 \sigma^3 + 1.1171 \sigma^2 - 28.21 \sigma + 758.85$	0.99	12.8	33.2
1150	0.01	$\theta = 0.1099 \sigma^3 - 12.765 \sigma^2 + 445.65 \sigma - 4093$	0.96	38.7	54.1
1150	0.1	$\theta = 0.0219 \sigma^3 - 3.5894 \sigma^2 + 168.26 \sigma - 1669.7$	0.99	54.6	76

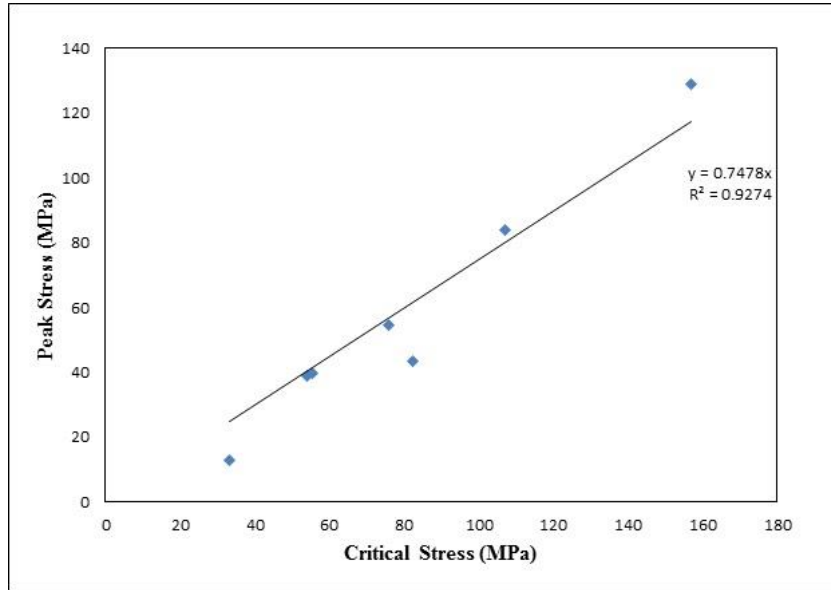


Fig. 5. Peak stress versus critical stress curve.

As stated before, the critical stress decreases with decreasing  $Z$  values due to better condition for initiation of DRX. Nearly similar value for normalized critical stress has been reported for austenitic stainless steels [16].

### 3.4. Constitutive equations approach

The correlation between the flow stress ( $\sigma$ ), temperature ( $T$ ), and strain rate ( $\dot{\epsilon}$ ), particularly at high temperatures, could be expressed by an Arrhenius-type constitutive equation. Further, the effects of temperature and strain rate on hot deformation behavior could be represented by the Zener-Holloman parameter ( $Z$ ) in an exponent-type equation [17,18]. These are mathematically expressed as:

$$Z = \dot{\epsilon} \exp\left(\frac{Q}{RT}\right) = A(\sinh(\alpha\sigma))^n \quad (5)$$

$$\dot{\epsilon} = AF(\sigma)\exp\left(-\frac{Q}{RT}\right) \quad (6)$$

where

$$\begin{aligned} F(\sigma) &= \sigma^n && \text{for } \alpha\sigma < 0.8 \\ &= \exp(\beta\sigma) && \text{for } \alpha\sigma > 1.2 \\ &= [\sinh(\alpha\sigma)]^n && \text{for all } \sigma \end{aligned}$$

Here,  $R$  is the universal gas constant ( $8.31 \text{ J mol}^{-1} \text{ K}^{-1}$ );  $T$  is the absolute temperature in  $K$ ;  $Q$  is the activation energy ( $\text{kJ mol}^{-1}$ ); and  $A$ ,  $\alpha$ ,  $\beta$ , and  $n$  are the materials constants,  $\alpha = \beta/n$ .

True stress- strain curves were obtained at three strain rates of  $0.1$ ,  $0.01$ , and  $0.001 \text{ s}^{-1}$  and at temperatures of  $950$ ,  $1050$  and  $1150 \text{ }^\circ\text{C}$ . Flow stress data from the compression tests (Fig. 1) at various deformation conditions were used to evaluate the material constants of the constitutive equations. The procedure for determination of material constants at a true strain of  $0.5$  is as follows. For low and high stress levels, substituting the value of  $F(\sigma)$  in Eq. (6), at constant temperature, gives the following corresponding expressions:

$$\dot{\epsilon} = B\sigma^n \quad (7)$$

$$\dot{\varepsilon} = C \exp(\beta\sigma) \quad (8)$$

where  $B$  and  $C$  are the material constants, depending on temperature. The logarithm form of both sides of Eq. 7 and 8 yields, respectively,

$$\ln \sigma = \frac{1}{n} \ln(\dot{\varepsilon}) - \frac{1}{n} \ln(B) \quad (9)$$

$$\sigma = \frac{1}{\beta} \ln(\dot{\varepsilon}) - \frac{1}{\beta} \ln(C) \quad (10)$$

The values of  $n$  and  $\beta$  can be obtained from the slope of the lines in the  $\ln \sigma$  versus  $\ln$  (strain rate) plot (Fig. 6) and  $\sigma$  versus  $\ln$  (strain rate) plot (Fig. 7), respectively.

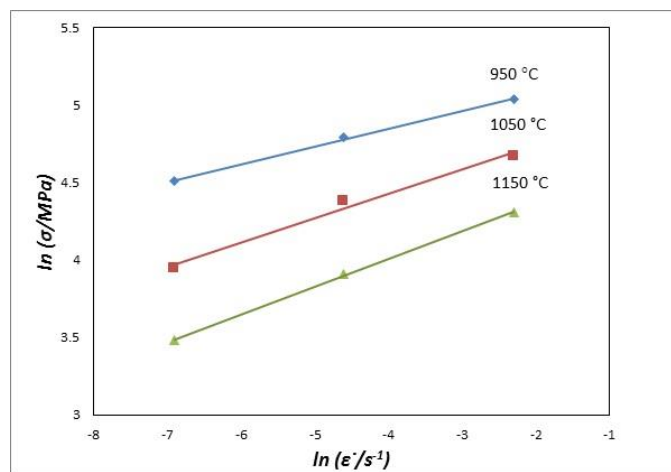


Fig. 6. Plot of  $\ln$  (stress) versus  $\ln$  (strain rate) to evaluate the value of  $n$ .

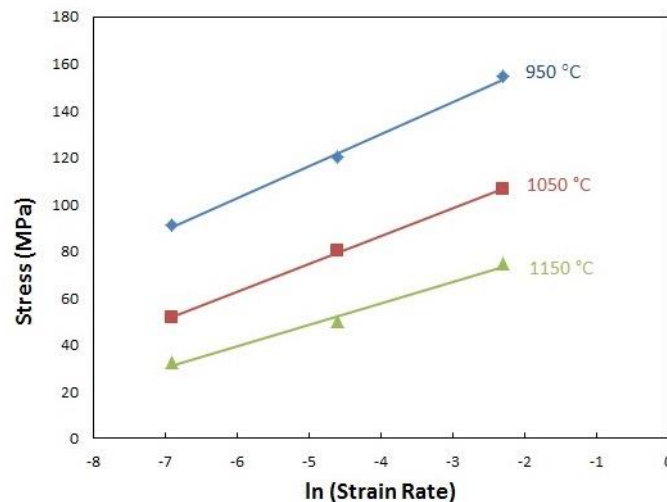


Fig. 7. Plot of stress versus  $\ln$  (strain rate) to evaluate the value of  $\beta$ .

It is apparent that the lines are almost parallel, leading us to observe that the slope of the lines consequently varies in a very small range. The slight variation in the slope of the lines could be attributed to scattering in the experimental data points. The inverse of mean value of the slopes was taken as the value of  $n$  and  $\beta$ , which was found to be 5.62 and  $0.086 \text{ MPa}^{-1}$ , respectively. This gives the value of  $\alpha = \beta/n = 0.0153$ .

For low as well as high stress levels, Eq. (6) can be written as:

$$\dot{\varepsilon} = A[\sinh(\alpha\sigma)]^n \exp\left(-\frac{Q}{RT}\right) \quad (11)$$

Taking the logarithm of both sides of Eq. (11) gives

$$\ln[\sinh(\alpha\sigma)] = \frac{\ln \dot{\varepsilon}}{n} + \frac{Q}{nRT} - \frac{\ln A}{n} \quad (12)$$

For a particular strain rate, differentiating Eq. (12) gives

$$Q = nR \frac{d\{\ln[\sinh(\alpha\sigma)]\}}{d\left(\frac{1}{T}\right)} \quad (13)$$

The value of  $Q$  can be derived from the slopes in a plot of  $\ln[\sinh(\alpha\sigma)]$  versus  $1/T$  (Fig. 8). The value of  $Q$  was determined by averaging the values of  $Q$  under different strain rates. At true strain of 0.5, the value of  $Q$  was found to be 334 kJ/mol. The value of  $A$  at a particular strain could be obtained by plotting the relationship between  $\ln Z$  versus  $\ln [\sinh(\alpha\sigma)]$ . As shown in Fig. 9, the value of  $A$  at 0.5 strain was found to be  $4.7 \times 10^{13}$ .

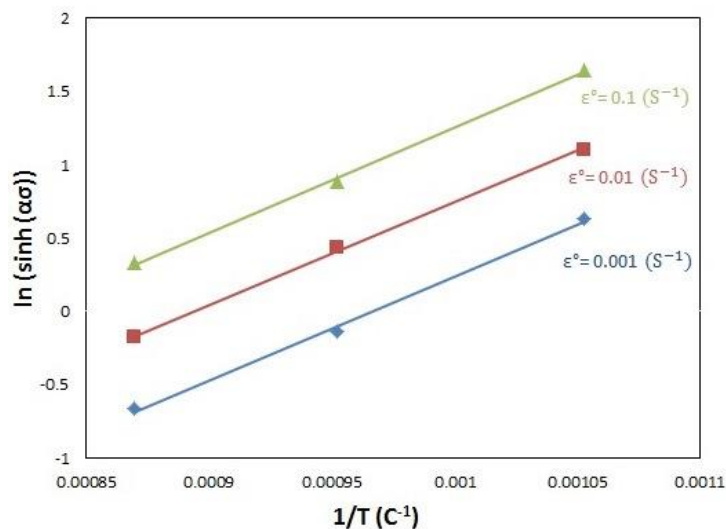


Fig. 8. Plot of  $\ln [\sinh(\alpha\sigma)]$  vs.  $(1/T)$  to estimate the value of  $Q$ .

Once the material constants are evaluated, the flow stress at a particular strain can be predicted. Considering Eqs. (5) and (11), the constitutive equation relating the flow stress and Zener- Holloman parameter can be written as;

$$\sigma = \frac{1}{\alpha} \sinh^{-1} \left( \frac{Z}{A} \right)^{\frac{1}{n}} \quad (14)$$

Figure 10 indicates the plot of the predicted stress versus experimentally measured stress at the strain of 0.5. It can be seen that the predicted values for stress are in a good agreement with experimentally measured ones. In addition, the correlation between steady state DRX grain sizes with Zener- Holloman parameter was depicted in Fig. 11. According to the aforementioned discussions, it is expected that the DRX grain size decreases with increasing Zener- Holloman parameter.

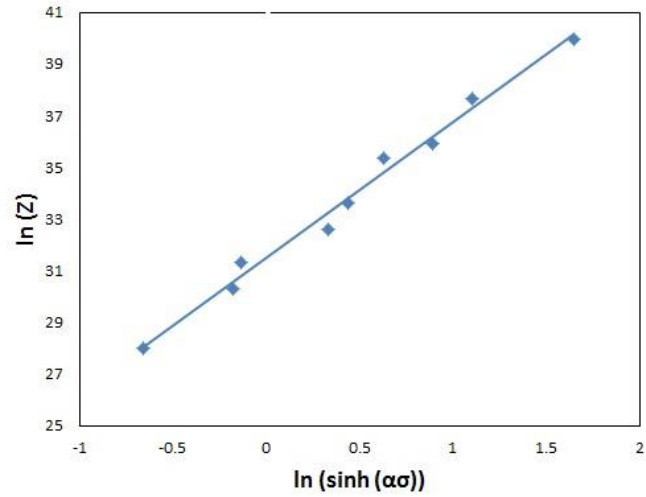


Fig. 9. Plot of  $\ln(Z)$  vs.  $\ln[\sinh(\alpha\sigma)]$  to estimate the value of  $A$ .

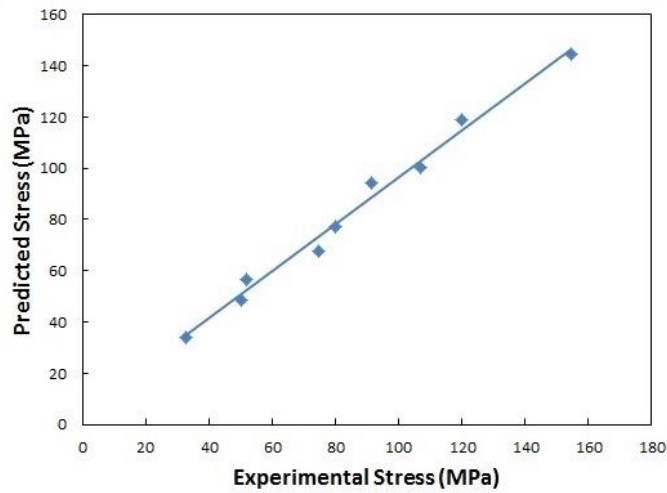


Fig. 10. Correlation between the experimental and predicted flow stress from sine hyperbolic constitutive equation at a strain of 0.5.

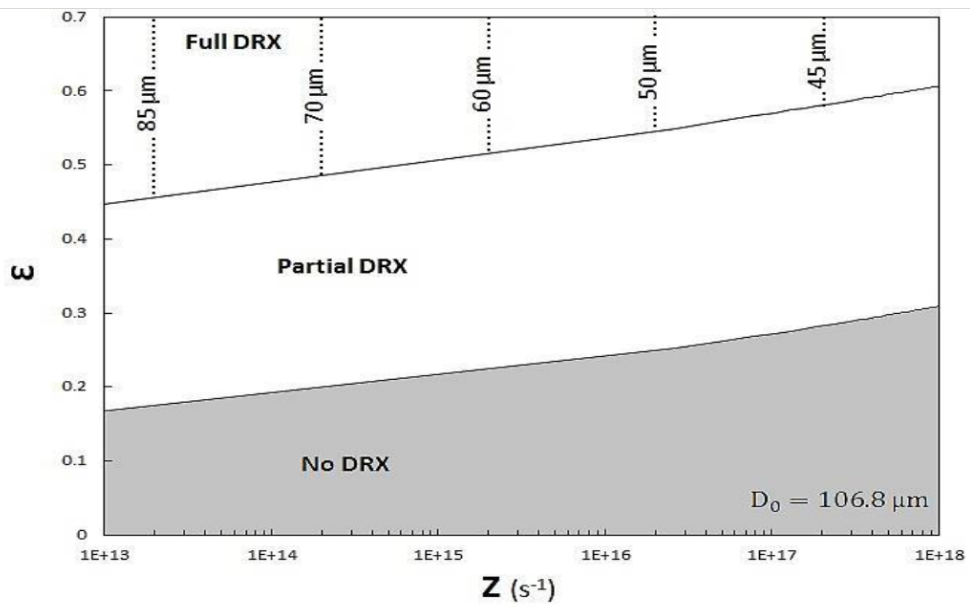


Fig. 11. Variations of DRX grain size with Zener- Holloman parameter.

#### 4. Conclusion

The following principal conclusions can be drawn from the present study:

- The stress- strain curves exhibited a typical DRX behavior with a single peak stress followed by a gradual fall towards a steady state stress.
- At high Z conditions, the DRX process of 17-7 PH stainless steel is very sluggish with the increase of strain due to co-existence of  $\delta$ - ferrite and high alloying elements.
- The normalized critical stress for initiation of DRX in 17-7 PH steel was found to be 0.74.
- Flow stress for 17-7 PH steel during hot working can be predicted well based on the sine hyperbolic type of constitutive equation relating stress and strain rate.

#### 5. References

- [1] H. Mirzadeh, M. H. Parsa and D. Ohadi, Hot deformation behavior of austenitic stainless steel for a wide range of initial grain size, *Mater. Sci. Eng., A*, 569 (2013) 54-60.
- [2] L. L. Wang, R. B. Li, Y. G. Liao and M. Jin, Study on characterization of hot deformation of 403 steel, *Mater. Sci. Eng., A*, 567 (2013) 84-88.
- [3] M. A. Mostafaei and M. Kazeminezhad, Hot deformation behavior of hot extruded Al-6Mg alloy, *Mater. Sci. Eng., A*, 535 (2012) 216-221.
- [4] H. Mirzadeh, J. M. Cabrera and A. Najafizadeh, Constitutive relationships for hot deformation of austenite, *Acta Mater.*, 59 (2011) 6441-6448.
- [5] E. Shafiei and K. Dehghani, Prediction of single-peak flow stress curves at high temperatures using a new logarithmic-power function, *J. Mater. Eng. Perform.*, 25(2016)4024-4035.
- [6] M. Marchattivar, A. Sarkar, J. K. Chakravarty and B. P. Kashyap, Dynamic recrystallization during hot deformation of 304 austenitic stainless steel, *J. Mater. Eng. Per.*, 22 (2013) 2168-2175.
- [7] C. M. Cepeda- Jimenez, O. A. Ruano, M. Carsi and F. Cerreno, Study of hot deformation of an Al-Cu-Mg alloy using processing maps and microstructural characterization, *Mater. Sci. Eng., A*, 552 (2012) 530-539.
- [8] A. Najafizadeh and J. J. Jonas, Predicting the critical stress for initiation of dynamic recrystallization, *ISIJ Int.*, 46 (2006) 1679-1684.
- [9] E. Shafiei and R. Ebrahimi, A modified model to estimate single peak flow stress curves of Ti-IF Steel, *ISIJ Int.*, 52 (2012) 569-573.
- [10] Y. Han, G. Liu, D. Zou, R. Liu and G. Qiao, Deformation behavior and microstructural evolution of as-cast 904L austenitic stainless steel during hot compression, *Mater. Sci. Eng., A*, 565 (2013) 342-350.
- [11] A. Dehghan- Manshadi and P. D. Hadgson, Effect of  $\delta$ -ferrite co-existence on hot deformation. and recrystallization of austenite, *J. Mater. Sci.*, 43 (2003) 6272-6277.
- [12] H. J. McQueen and N. D. Ryan, Constitutive analysis in hot working, *Mater. Sci. Eng., A*, 322 (2002) 43-47.
- [13] E. Shafiei and R. Ebrahimi, A new constitutive equation to predict single peak flow stress curves, *J. Eng. Mater. Tech.*, 135 (2013) 011006- 4.
- [14] H. Mirzadeh and A. Najafizadeh, The rate of dynamic recrystallization in 17-4 PH stainless steel, *Mater. Des.*, 31 (2010) 4577- 4583.
- [15] E. I. Poliak and J. J. Jonas, Critical strain for dynamic recrystallization in variable strain rate, *ISIJ Int.*, 43 (2003) 692- 700.
- [16] H. Mirzadeh and A. Najafizadeh, Prediction of the critical conditions for initiation of dynamic recrystallization, *Mater. Des.*, 31 (2010) 1174- 1179.
- [17] A. Etaadi and K. Dehghani, *Mater. Chem. Phy.*, A study on hot deformation behavior of Ni-42.5 Ti-7.5 Cu alloy, 140 (2013) 208- 215.
- [18] H. Y. Wu, J. C. Yang, F. J. Zhu and C. T. Wu, Hot compressive flow stress modeling of homogenized AZ61 Mg alloy using strain-dependent constitutive equation, *Mater. Sci. Eng., A*, 574 (2013) 1724- 1726.

## رفتار تغییر فرم گرم فولاد زنگ نزن 17-7PH

محمد زینلی<sup>1</sup>، احسان شفیعی<sup>2</sup>، رضا حسینی<sup>3</sup>، خسرو فرمنش<sup>1</sup>، عبدالرضا سلطانی پور<sup>1</sup>، اسماعیل مقصودی<sup>1</sup>

<sup>1</sup> دانشکده علم و مهندسی مواد، دانشگاه صنعتی مالک اشتر، شاهین شهر، اصفهان.

<sup>2</sup> دانشکده معدن و متالورژی، دانشگاه صنعتی امیرکبیر، تهران، ایران.

<sup>3</sup> گروه علم و مهندسی مواد، دانشکده فنی و مهندسی، دانشگاه شیراز، شیراز، ایران.

**چکیده:** جهت بررسی رفتار تغییر فرم گرم فولاد زنگ نزن 17-7PH، آزمایشات فشار گرم در دماهای  $950^{\circ}\text{C}$ ،  $1050^{\circ}\text{C}$  و  $1150^{\circ}\text{C}$  و نرخ کرنش های 0/001 تا 0/1 بر ثانیه انجام شد. بر این اساس رفتار تغییر فرم گرم با بهره گیری از نمودارهای تنش سیلان، نمودارهای نرخ کار سختی بر حسب تنش سیلان، معادلات ساختاری توانی و ریزساختار مورد مطالعه قرار گرفت. همچنین تنش بحرانی برای شروع تبلور مجدد دینامیکی با استفاده از توابع نمایی درجه سوم محاسبه گردید. نتایج نشان می دهد که تنش سیلان وابستگی زیادی به دمای تغییر فرم و نرخ کرنش دارد. بطوری که تنش سیلان با افزایش نرخ کرنش و کاهش دمای تغییر فرم افزایش پیدا می کند. بعلاوه اثبات شد که حضور فاز فریت دلتا منجر به کاهش نرخ نرم شدگی در نرخ کرنش های بالا و دماهای پایین می شود. نتایج بدست آمده تطابق بسیار خوبی را بین پیش بینی های معادلات ساختاری و نتایج تجربی نشان می دهد.

**واژگان کلیدی:** تغییر فرم گرم؛ تبلور مجدد دینامیکی؛ معادلات ساختاری؛ فولاد زنگ نزن 17-7PH.